Supplementary material

Unveiling the deformability of mussel plaque core: the role of pore distribution and hierarchical structure

Yulan Lyu[a,b], Mengting Tan[c], Yong Pang[b], Wei Sun[a] , Shuguang Li[a] and Tao Liu[b,*]

[a]Faculty of Engineering, University of Nottingham, Nottingham NG7 2RD, UK;
[b]School of Engineering and Materials Science, Queen Mary University of London, London E1 4NS, UK;
[c]School of Mechanical Engineering, Nanjing University of Science and Technology, Nanjing 210094, Jiangsu, China

Corresponding Authors*: tao.liu@qmul.ac.uk

KEYWORDS: Biomechanics, blue mussel, mussel plaque, phase field model, 3D printing, random porous structures, hyperelasticity

S1: The pore distribution analysis of mussel plaque SEM photos

Figs. S1 and S2 were analysed with additional SEM images to further investigate the pore distribution of large-scale pores within mussel plaques. It can be concluded that the large-scale pore radius still follows lognormal distribution. The porosity (^{v_l}), normalised mean radius ($\bar{\mu}^*_p$) and normalised standard deviation of radius ($\bar{s}^*_p$) for large-scale pores within those SEM images are shown in table S1 and S2, respectively.

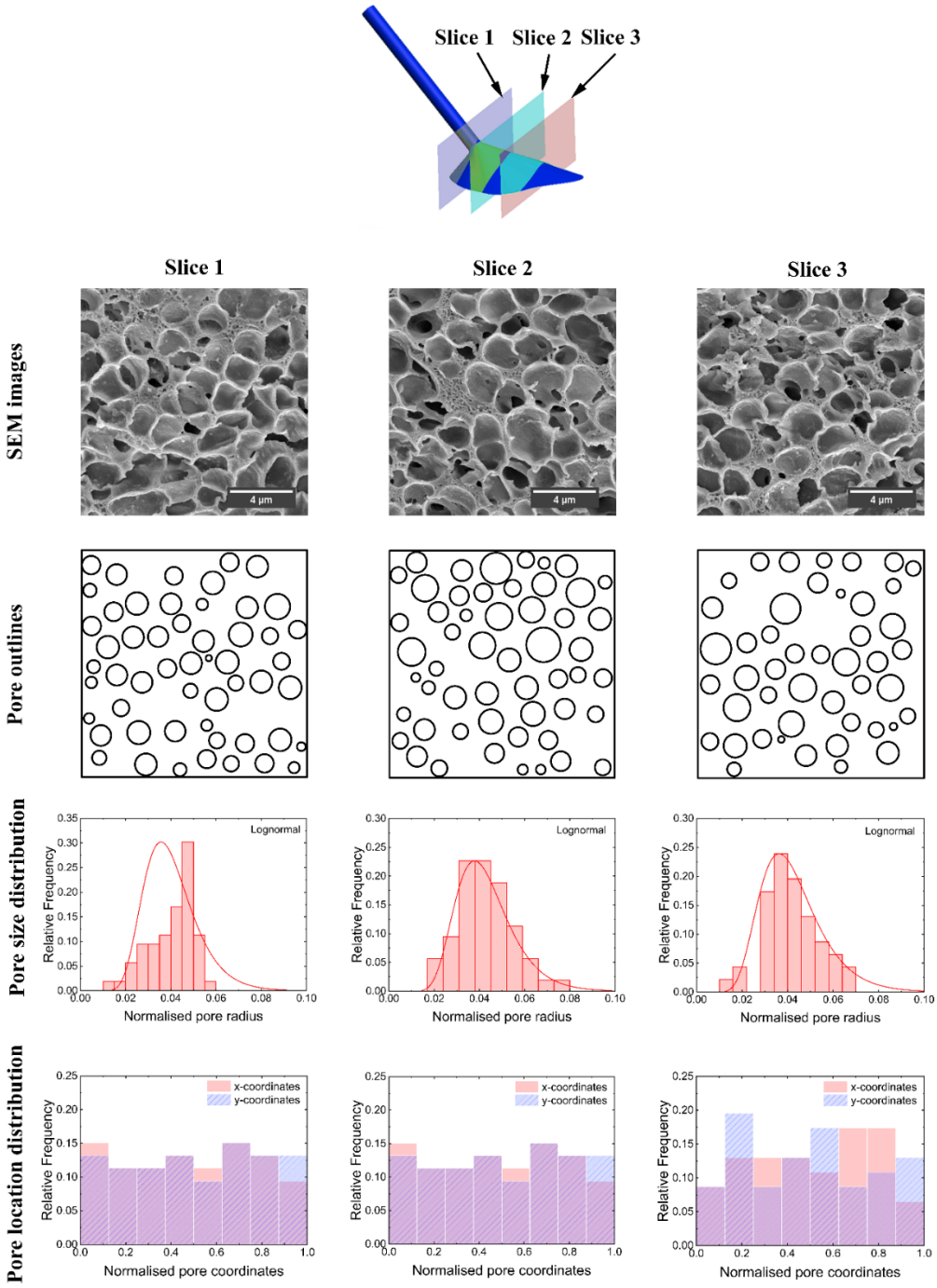

Figure S1: Large-scale pore size and location distribution analysis for SEM images of the same mussel.

Table S1. Porosity (v_l), normalised mean radius ($\bar{\mu}_p^*$) and normalised standard deviation of radius ($\bar{s}_p^*$) of simplified large-scale pores within the SEM images of the same mussel.

	Porosity (v_l)	$\bar{\mu}_p^*$	$\bar{s}_p^*$
Slice 1	33%	0.043	0.012
Slice 2	28%	0.039	0.008
Slice 3	27%	0.041	0.012

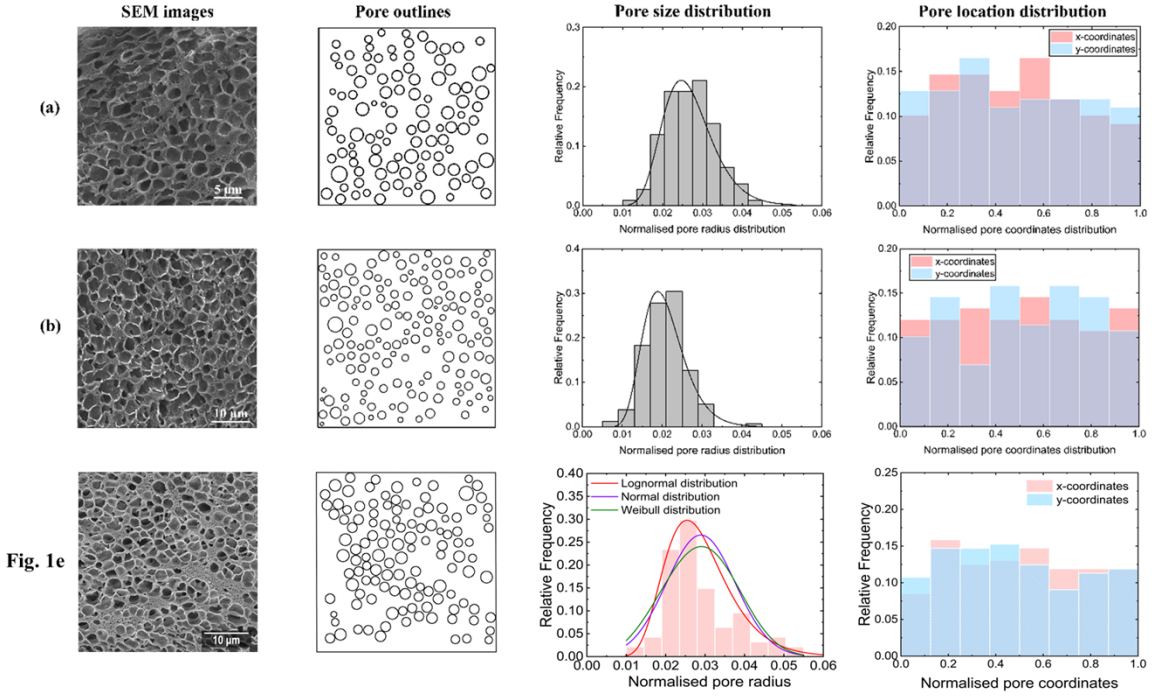

Figure S2: Large-scale pore size and location distribution analysis for SEM images of different mussel plaques.

Table S2. Porosity (v_l), normalised mean radius ($\bar{\mu}_p^*$) and normalised standard deviation of radius ($\bar{s}_p^*$) for simplified large-scale pores within the SEM images.

	Porosity (v_l)	$\bar{\mu}_p^*$	$\bar{s}_p^*$
Figure S2a	26%	0.027	0.006
Figure S2b	23%	0.021	0.005
Figure 1e	27%	0.031	0.009

S2: The simplified process of the pore distribution of the mussel plaque cores

The porous structure of the mussel plaque is inherently complex, with irregular pores varying significantly in shape and size, posing challenges for accurate quantification of porosity and other distribution parameters. To address this, we have idealised these irregular pores into circular shapes, enabling a more straightforward approach to measuring key parameters such as porosity, pore radius, and the coordinates of pore centres (Fig. S3). This idealisation ensures uniformity in analysis and facilitates the application of mathematical models and computational methods. During this process, pores that appeared incomplete or have poorly defined boundaries were excluded in order to maintain the accuracy and reliability of the measurements. Special attention was given to avoid overlap of pores during the idealisation process, as overlapping can lead to incorrect calculations of porosity and pore distribution. Despite the simplification to circular pores, the main geometrical features of the mussel plaque are retained, ensuring the pore arrangement remains consistent with the original complex structure.

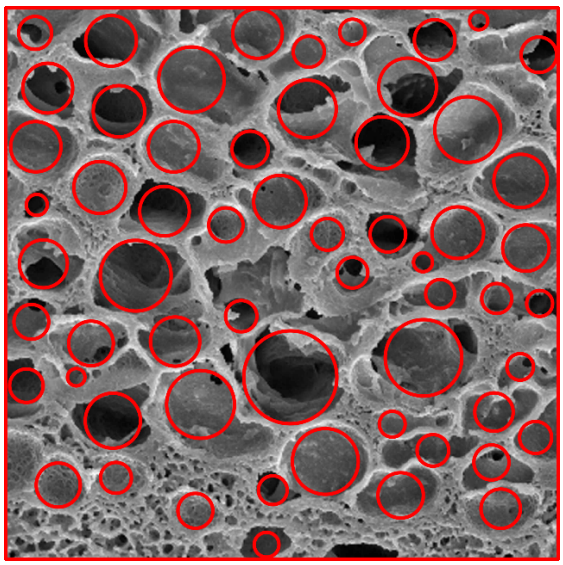

Figure S3: The schematic drawing of the idealisation of the porous structure of mussel plaque cores.

S3: The Q–Q (quantile–quantile) plots

The Q–Q (quantile–quantile) plot [1], which serves as a probability plot, was drawn in Fig. S4 to compare the probability distributions of x and y coordinates of the centers of large-scale pores in those 9 SEM images to a uniform distribution.

It can be seen that both x and y coordinates are consistent to a uniform distribution. Therefore, a uniform distribution of large-scale pores locations was applied to generate the porous RVEs.

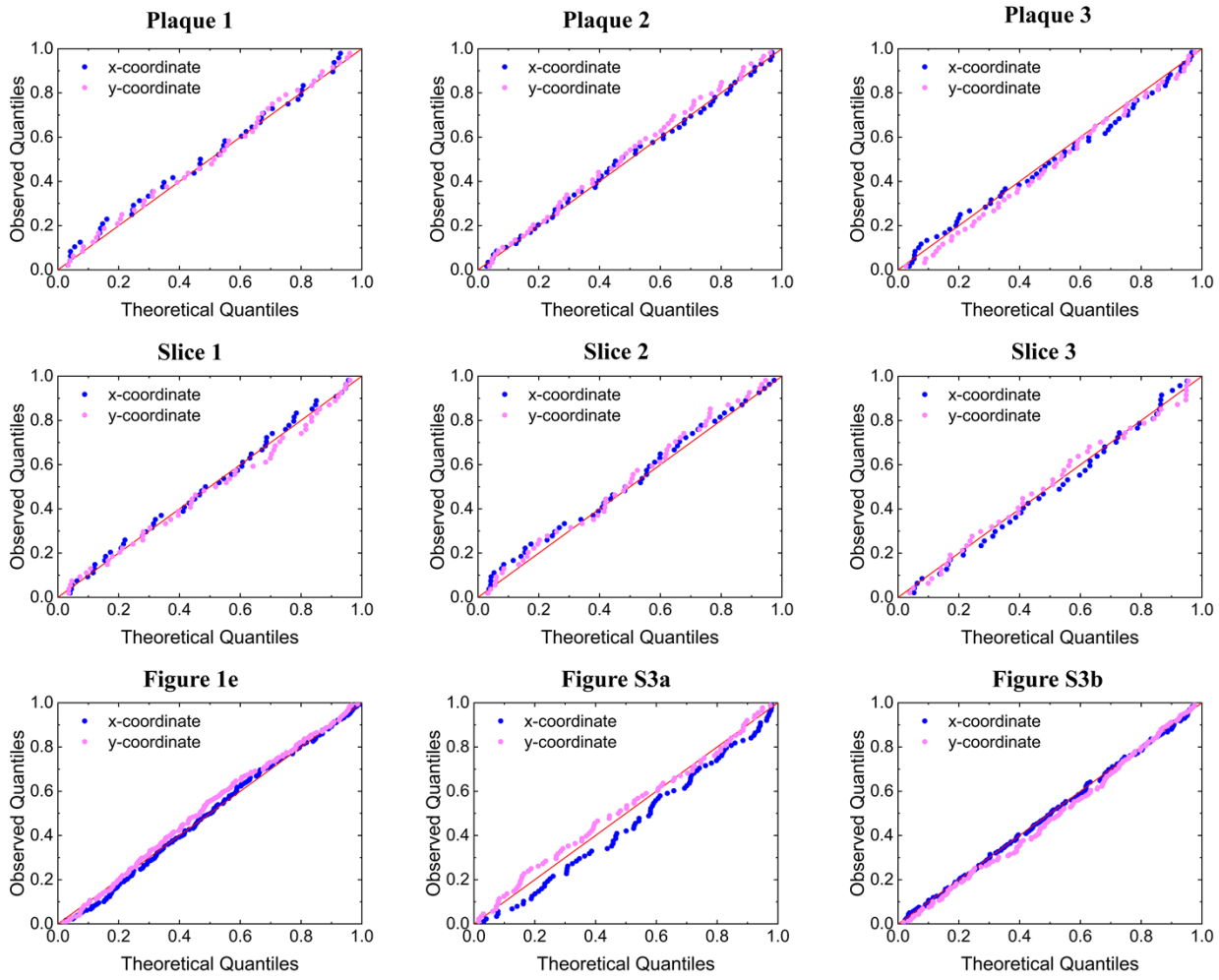

Figure S4: Q–Q plots (quantile–quantile plot) comparing the x and y coordinates of large pores within the 9 mussel plaque SEM photos to a uniform distribution.

S4: The size effect study of RVE

Because the random distribution of pores itself has an effect on the stress-strain curve of the RVE, the use of randomly distributed pore samples to detect dimensional effects is not applicable. Instead, pores with a radius of 1.12 mm (mean value of pore size distribution) were uniformly arranged in RVEs of three different sizes (15x15 mm, 30x30 mm, 60x60 mm). The porosity of the RVEs of all sizes was 27%, which is the same as before. In order to ensure that the pore spacing was equal for each of the three different RVE sizes, a spacing of 3.66 mm was applied (Fig. S5).

It can be seen from Fig. S6 that the stress-strain curves of the three different sizes of RVEs almost overlap, thus learning that the size effect can be neglected in this study. The 30x30 mm RVE size was chosen based on the computational power and the similarity of pore numbers.

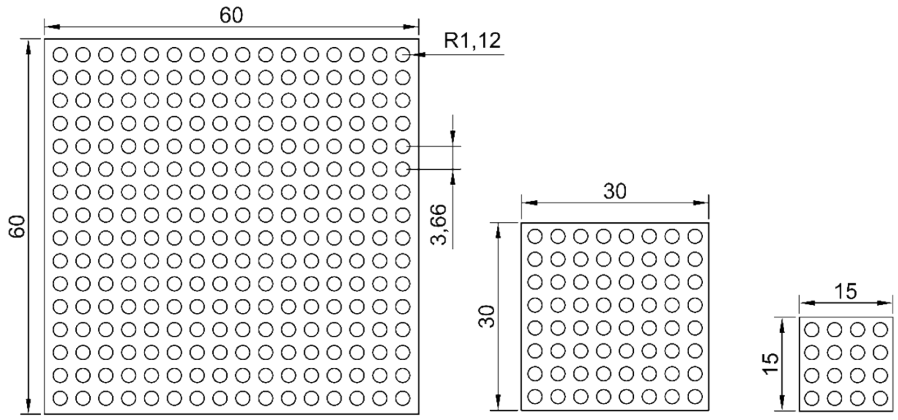

Figure S5: Schematic diagram of three different sizes RVEs (60x60 mm, 30x30 mm, 15x15 mm).

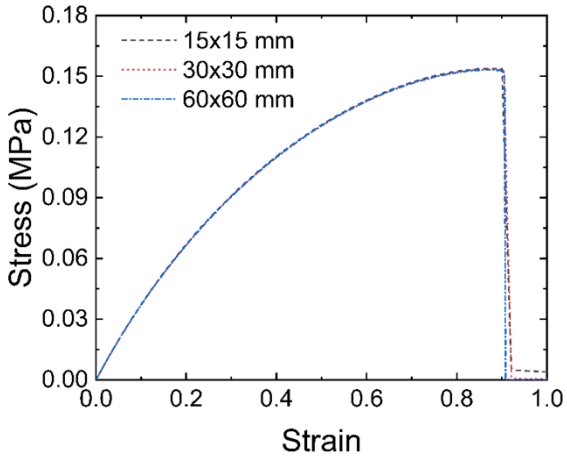

Figure S6: Strain-stress curves of three different sizes RVEs (60x60 mm, 30x30 mm, 15x15 mm).

S5: The small-scale pores size effect study for the multi-scale porous RVEs

Sample C in Section 5.2 was selected to regenerate the multi-scale porous RVEs with three different approximate small-scale pore sizes (0.4 mm, 0.5 mm and 0.6 mm) to understand the size effect on the macroscopic material behaviours of multi-scale RVEs. In ABAQUS, Sample C was meshed using triangular elements with three different approximate mesh sizes: 0.4 mm, 0.5 mm and 0.6 mm. The 2D elements in the FE models were then removed and the remaining nodes were connected using truss elements (T2D2T) as described in Section 3.2 of the original text. This generated three multi-scale porous RVEs with approximate small-scale pore size approximations of 0.4 mm, 0.5 mm and 0.6 mm respectively. It is noteworthy that the porosities of these three multiscale porous RVEs remain consistent by adjusting the radius of truss elements.

The results show that the size of the small-scale pores within the multi-scale porous RVEs has an insignificant effect on the macroscopic material behaviours of multi-scale porous RVEs thereby 0.5 mm was set as the approximate small-scale pore size in the simulations (Fig. S7).

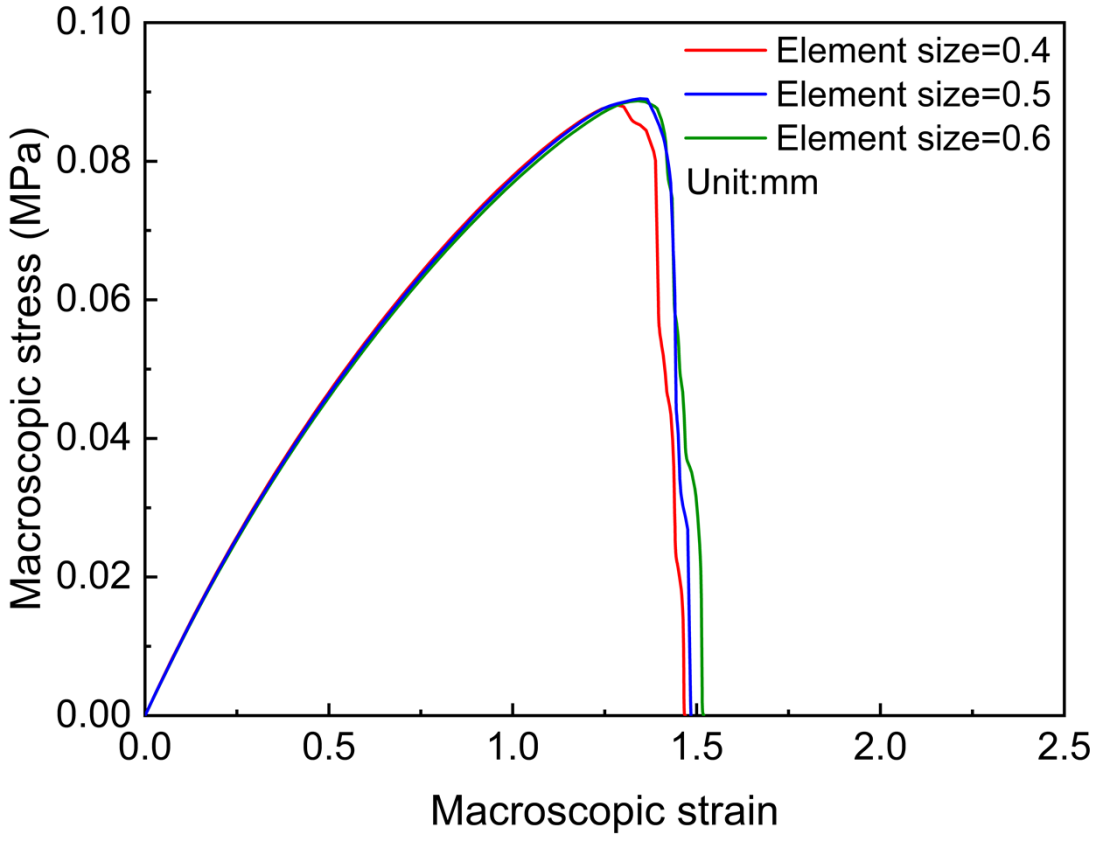

Figure S7: The macroscopic stress-strain curves of multi-scale porous RVEs with different approximate small-scale pore sizes: 0.4 mm, 0.5 mm (Sample C') and 0.6 mm.

S6: The derivation of eqn (14)

The following equation can be derived from eqns (12) and (13) in the original text:

$$\dot{U} = \int_{\Omega} \left(\frac{\partial g(c)}{\partial c} \dot{\psi c} + g(c) \frac{\partial \psi}{\partial F} : \dot{F} \right) dV \qquad (S6.1)$$

where $\dot{F}$ is the rate of change of the deformation gradient, which can be presented as $\dot{F} = \frac{d}{dt}(\nabla u) = \nabla \frac{du}{dt} = \nabla \dot{u}$. The velocity field $\dot{u}$ represents the rate of change of the displacement field u with respect to time.

Meanwhile, the vector calculus identity for the divergence of a product of a vector field a and a vector field A is shown below:

$$\text{div}\,(a \cdot A) = a \cdot \text{div}\,(A) + A : \nabla a \qquad (S6.2)$$

Therefore, the second term on the right-hand side of eqn (S6.1) can be written as:

$$\int_{\Omega} g(c) \frac{\partial \psi}{\partial F} : \dot{F}\, dV = \int_{\Omega} g(c) \frac{\partial \psi}{\partial F} : \nabla \dot{u}\, dV = \int_{\Omega} div \left(g(c) \frac{\partial \psi}{\partial F} \cdot \dot{u} \right) dV - \int_{\Omega} div \left(g(c) \frac{\partial \psi}{\partial F} \right) \cdot \dot{u}\, dV \qquad (S6.3)$$

It is also known that the equation of the divergence theorem is,

$$\int_{\Omega} \nabla \cdot F dV = \int_{\partial \Omega} F \cdot n dA \qquad (S6.4)$$

Hence eqn (S6.3) can be rewritten as:

$$\int_{\Omega} g(c) \frac{\partial \psi}{\partial F} : \dot{F}\, dV = \int_{\partial \Omega} g(c) \frac{\partial \psi}{\partial F} \cdot \dot{u} \cdot n dA - \int_{\Omega} \left(\nabla \cdot \left(g(c) \frac{\partial \psi}{\partial F} \right) \right) \cdot \dot{u}\, dV \qquad (S6.5)$$

Consequently, eqn (S6.1) can be expressed as:

$$\dot{U} = \int_{\Omega} \left(\frac{\partial g(c)}{\partial c} \dot{\psi c} \right) dV + \int_{\partial \Omega} g(c) \frac{\partial \psi}{\partial F} \cdot \dot{u} \cdot n dA - \int_{\Omega} \left(\nabla \cdot \left(g(c) \frac{\partial \psi}{\partial F} \right) \right) \cdot \dot{u}\, dV \qquad (S6.6)$$

S7: The derivation of eqn (18)

Based on eqn (17) in the original text, the rate of the dissipated energy from crack formation $\dot{D}^f$ can be expressed as:

$$\dot{D}^f = \int_\Omega G_c\left(\frac{c\dot{c}}{l} + l(\nabla c \cdot \nabla \dot{c})\right)dV \quad (S7.1)$$

The vector calculus identity for the divergence of a product of a scalar field ϕ and a vector field A is shown below:

$$\nabla \cdot (\phi A) = \nabla\phi \cdot A + \phi(\nabla \cdot A) \quad (S7.2)$$

Therefore, the second term on the right-hand side of eqn (S6.1) can be rewritten as:

$$\int_\Omega (G_c l \nabla c \cdot \nabla \dot{c}))dV = \int_\Omega \nabla \cdot \left(G_c l \nabla c \dot{c}\right)dV - \int_\Omega G_c \dot{l} c(\nabla \cdot \nabla c)dV \quad (S7.3)$$

Meanwhile, the equation of the divergence theorem is shown below,

$$\int_\Omega \nabla \cdot F dV = \int_{\partial\Omega} F \cdot n dA \quad (S7.4)$$

Thus eqn (S7.3) can be rewritten as follow:

$$\int_\Omega (G_c l \nabla c \cdot \nabla \dot{c}))dV = \int_{\partial\Omega} G_c l \nabla c \dot{c} \cdot n dA - \int_\Omega G_c \dot{l} c(\nabla \cdot \nabla c)dV \quad (S7.5)$$

Finally, based on eqns (S7.1) and (S7.3), we can obtain the following equation:

$$\dot{D}^f = \int_\Omega G_c \dot{c}\left(\frac{c}{l} - l\nabla^2 c\right)dV + \int_{\partial\Omega} G_c l \nabla c \dot{c} \cdot n dA \quad (S7.6)$$

S8: The comparison of the solid and small-scale porous RVEs

Following Section 5.3, a small-scale porous RVE with 5% porosity, reflecting the porosity of small-scale pores observed in the plaque SEM image (Fig. 1e), was firstly generated to compare with the solid RVE and study the effect of the small-scale porous structure on material stiffness. It can be seen from Fig. S8 that the solid RVE exhibited significantly higher stiffness compared to the small-scale porous RVE. This indicates that even with a relatively small amount of porosity, the microstructure can substantially impact the mechanical properties, reducing the stiffness and making the material more compliant under tensile loading.

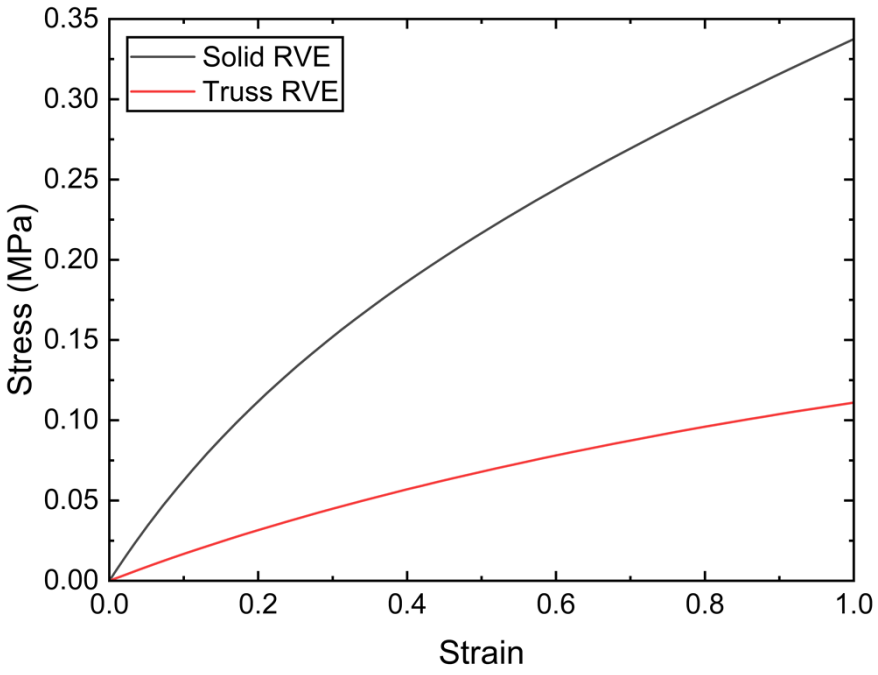

Figure S8: The stress-strain curves of the solid and small-scale porous RVEs.

References

[1] Wilk, M.B. and Gnanadesikan, R., 1968. Probability plotting methods for the analysis for the analysis of data. Biometrika, 55(1), pp.1-17.